



A strength implicit correction scheme for the viscous-plastic sea ice model

Jennifer K. Hutchings^{a,*}, Hrvoje Jasak^b, Seymour W. Laxon^c

^a *International Arctic Research Center, University of Alaska: Fairbanks, 903 Koyukuk Dr., Fairbanks, AK 99775-7320, USA*

^b *Nabla Ltd., The Mews, Picketts Lodge, Picketts Lane, Salfords, Surrey RH1 5RG, UK*

^c *Centre for Polar Observation and Modelling, University College London, London WC1E 6BT, UK*

Abstract

With increasing awareness of the role of the polar regions in global climate, efficient and accurate simulation of sea ice is an important issue. The numerical solution procedure for the viscous-plastic sea ice model is examined. Recent developments are drawn upon and new discretisation practices introduced that improve efficiency and the accuracy of the simulation. The main components of the new solution procedure are bounded and conservative finite volume discretisation and a reinterpretation of the model structure, including the introduction of a method to resolve momentum-ice strength coupling. It is found that traditional segregated momentum solution procedures do not ensure mass conservation, which may introduce substantial thickness errors in Arctic sea ice simulations. The strength implicit correction scheme ensures mass conservation for a similar computational expense as previous, non-conservative methods.

© 2003 Elsevier Ltd. All rights reserved.

1. Introduction

Sea ice is an important component of the polar climate. In the Northern Hemisphere it modulates the ocean–atmosphere interaction, transports fresh water into the Greenland–Iceland–Norwegian (GIN) Sea and maintains Arctic Ocean stratification. In the Antarctic coastal seas, in particular the Weddell Sea, sea ice contributes to the formation of Antarctic Deep and Bottom Water. Modelling these processes requires accurate diagnostic of ice mass, lead fraction and ice motion. Sea ice models with an elliptical viscous-plastic constitutive relation are found to reproduce observed ice drift well in comparison with models that do not include shear viscosity

* Corresponding author. Tel.: +1-907-474-7569; fax: +1-907-474-2643.

E-mail addresses: jenny@iarc.uaf.edu (J.K. Hutchings), h.jasak@nabla.co.uk (H. Jasak).

(Kreyscher et al., 2000). Hence there is interest in including this model in global climate models and in studies of oceanic circulation with coupled ice-ocean models (Lemke et al., 1998). Currently, the viscous-plastic model is being included in the Hadley Centre Climate Model (priv. comm. Doug Cresswell) and the Community Climate System Model (Bitz et al., 2001).

We focus our attention on accurate, stable and efficient discretisation of the viscous-plastic model with elliptical rheology (Hibler, 1979), hereafter referred to as the Hibler model. The original doubly-staggered finite difference (FD) scheme used to numerically simulate the sea ice behaviour was considered state-of-the-art when the model was first published. More recently segregated solutions (Oberhuber, 1993; Zhang and Hibler, 1997) have been introduced, though these still use a staggered FD scheme. Hunke and Dukowicz (1997) introduced an elastic–viscous-plastic (EVP) formulation of the Hibler model, allowing a fully explicit numerical scheme which has similar computational efficiency as segregated implicit schemes. The EVP model is proving popular in global climate models as its explicit formulation enables straight forward parallelisation of the code. This paper draws upon recent advances in the field of computational fluid dynamics (CFD) and, more generally, computational continuum mechanics (CCM) to improve the numerics behind the Hibler model. A segregated implicit approach is taken, allowing the use of efficient sparse matrix solvers for expedient solution of problems with many discretisation elements (Ferziger and Perić, 1995). The parallelisation of these matrix solvers has been optimised (Kaluderčić, 2000), and is implemented in the code used to produce results in this paper (Weller et al., 1998)¹. We expect a similar, if not better, computational performance compared to the EVP algorithm.

Modern discretisation practices can be broadly divided into two groups: the finite element method (FEM), ruling supreme in the field of structural analysis and solid mechanics and the finite volume method (FVM), prevalent in the simulation of fluid flows and highly non-linear phenomena. In this paper the finite volume (FV) discretisation of the Hibler model is presented, bringing several important numerical improvements:

- strict conservation of ice mass;
- greater freedom in mesh generation, particularly allowing for locally increased mesh resolution through embedded mesh refinement;
- separation of the elliptic model effects through the stress state and
- accurate resolution of non-linear ice interaction.

To achieve the above, we draw on the well-established practices from the fields of CFD and CCM; the first step in this being the “reinterpretation” of the model itself.

In Section 2 the viscous-plastic rheology model is summarised and some general statements on its characteristics are made. We demonstrate that this model is remarkably similar in its nature to a combination of a supersonic flow model and a non-linear (solid) stress model. Section 3 gives a short summary of the FV discretisation, followed by the algorithmic “tricks” typically associated with the FV modelling of supersonic flow and linear stress analysis. In Sections 5 and 6 we formulate the FV equivalent of the Zhang and Hibler (1997) numerics, introduce the new strength implicit correction scheme and compare the two solution algorithms. The rest of the paper is

¹ Nabla Ltd. Web site <http://www.nabla.co.uk>

devoted to the comparison of the two models in terms of numerical accuracy, efficiency and convenience. In conclusion, we review the new discretisation practice and offer a set of guidelines for its application to other similar sea ice rheology models.

2. Model description

The viscous-plastic sea ice model was originally developed by Hibler (1979). For daily time scales the momentum balance is taken to be

$$\frac{\partial(m\mathbf{u})}{\partial t} + \nabla \cdot (m\mathbf{u}\mathbf{u}) = \mathbf{F} + \nabla \cdot \boldsymbol{\sigma}, \tag{1}$$

where m is the ice mass per unit area, \mathbf{u} is ice velocity and \mathbf{F} is the sum of body and surface forces on the ice, including the wind stress and ocean stress on the ice surface, Coriolis force and the pressure gradient force arising from the horizontal variations of the sea-surface elevation. The force due to sub-grid scale ice interaction, $\nabla \cdot \boldsymbol{\sigma}$, is highly non-linear and must be considered carefully in the numerical solution. The ice stress $\boldsymbol{\sigma}$ is modelled as a viscous-plastic material obeying the associated flow rule and an elliptical yield criterion (Hibler, 1979), Fig. 1

$$\boldsymbol{\sigma} = \eta[\nabla\mathbf{u} + \nabla\mathbf{u}^T] + [(\zeta - \eta)\mathbf{I}\text{tr}(\nabla\mathbf{u})] - \mathbf{I}\frac{P}{2}, \tag{2}$$

where the bulk (ζ) and shear (η) viscosities are given by

$$\zeta = \frac{P}{2\Delta}, \tag{3}$$

$$\eta = \frac{\zeta}{e^2} \tag{4}$$

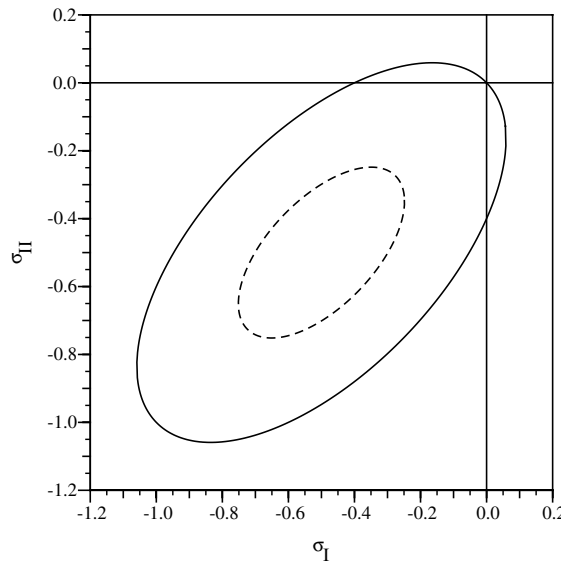


Fig. 1. Elliptical yield curve. The dashed ellipse demonstrates stress states invoked by the viscous closure scheme for small strain rates.

and Δ is defined as

$$\Delta = \left[\text{tr}(\dot{\hat{\epsilon}})^2 + \frac{2}{e^2} \dot{\hat{\epsilon}} : \dot{\hat{\epsilon}} \right]^{1/2}. \quad (5)$$

Here, e is the ratio of semi-major to semi-minor axes of the elliptical yield curve, P is the ice strength, $\dot{\hat{\epsilon}} = \frac{1}{2}[\nabla \mathbf{u} + (\nabla \mathbf{u})^T]$ is the strain rate, \mathbf{I} is the identity matrix and $\mathbf{q} : \mathbf{q}$ represents the scalar product of two second-rank tensors.

Ice mass continuity is described by the transport equations for effective ice thickness, $h = \frac{m}{\rho_i}$ where ρ_i is ice density, and the ice fraction A . Here a two level thickness model (Hibler, 1979) is used and the sources of ice thickness, S_h , and area, S_A , are calculated from climatological growth/melt rates (Thorndike et al., 1975)

$$\frac{\partial h}{\partial t} + \nabla \cdot (h\mathbf{u}) = S_h, \quad (6)$$

$$\frac{\partial A}{\partial t} + \nabla \cdot (A\mathbf{u}) = S_A. \quad (7)$$

To close the system of equations P must be determined. An empirical relationship for ice strength of the two level model is given by Hibler (1979)

$$P = P^* h e^{-C(1-A)}. \quad (8)$$

The model parameters are set to: $e = 2$, $C = 20$ and $P^* = 1 \times 10^4 \text{ N m}^{-1}$.

Before continuing with the analysis of boundedness (Section 4.1) and coupling (Section 4.4) in the discretised Hibler model, we review the basics of the FV discretisation in the following section. A more detailed discussion of this numerical solution technique may be found in Hutchings (2000).

3. Finite volume discretisation

Numerical discretisation of a particular equation set consists of two steps. First, the solution domain is decomposed into discrete space and time intervals, which do not overlap and completely cover the domain. The variation of the variable over each region is then prescribed; in our case, this is a linear function, creating a second-order accurate discretisation.

Consider the standard form of the transport equation for a general tensorial property ϕ

$$\frac{\partial \phi}{\partial t} + \nabla \cdot (\mathbf{u}\phi) - \nabla \cdot (\gamma \nabla \phi) = S_\phi(\phi, \dots), \quad (9)$$

where, without the loss of generality, the source term is linearised

$$S_\phi = S + L\phi. \quad (10)$$

Here, S and L may be a function of ϕ and/or any other solution parameters and $L < 0$. The solution of Eq. (9) may be iterated upon to achieve convergence over any non-linearity in S and L . The FVM of discretisation uses the integral form of the above equation over a control volume (CV), with a volume V_P and a computational point P in its centroid, Fig. 2

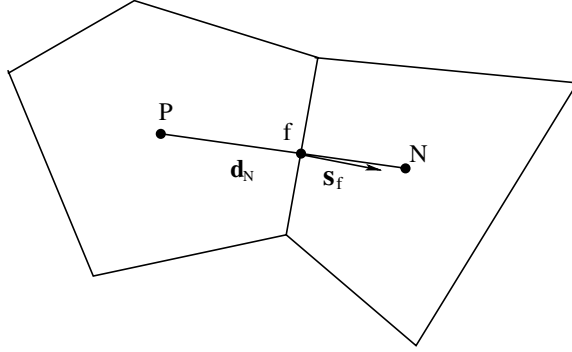


Fig. 2. A typical CV: \mathbf{s}_f is the face area vector for one face, \mathbf{d}_N is the vector between two neighbouring CV centres P and N around the face f .

$$\frac{d}{dt} \int_{V_p} \phi dV + \int_{V_p} \nabla \cdot (\mathbf{u}\phi) dV - \int_{V_p} \nabla \cdot (\gamma \nabla \phi) dV = \int_{V_p} S_\phi(\phi) dV. \tag{11}$$

The divergence terms in Eq. (11) are transformed into surface integrals using the generalised form of Gauss’ theorem. Second-order accurate approximation of the integrals in Eq. (11) is obtained by prescribing a linear variation of ϕ around P .

The temporal derivative is calculated using the Euler implicit method

$$\frac{\partial \phi}{\partial t} \approx \frac{\phi_P^n - \phi_P^0}{\delta t}, \tag{12}$$

where $\phi^n = \phi(t + \delta t)$, $\phi^0 = \phi(t)$ and δt is the time step. The non-linearity of the viscous-plastic model introduces a Courant number limitation. Experience shows that an efficient Courant number is of the order 0.5, which gives sufficiently accurate first-order time discretisation with the benefit of preserving boundedness.

The volume integrals are evaluated to second-order using the mid-point rule

$$\int_V \phi dV \approx \phi_P V_P, \tag{13}$$

where ϕ_P represents the value of ϕ in the centroid of the CV and V_P is its volume.

The surface integrals are split into the sum of integrals over the cell faces and approximated with the mid-point rule. For the advective term

$$\oint_S \mathbf{ds} \cdot \mathbf{u}\phi \approx \sum_f \mathbf{s}_f \cdot \mathbf{u}_f \phi_f = \sum_f F \phi_f, \tag{14}$$

where the ϕ_f is the value of ϕ interpolated to the face from the values at adjacent cell centres, \mathbf{s}_f is the outward-pointing face area vector, Fig. 2, and F is the face flux, defined for every cell face as

$$F = \mathbf{s}_f \cdot \mathbf{u}_f. \tag{15}$$

Boundedness of the discrete form of the convection term is achieved with a bounded second-order accurate differencing scheme (e.g. Jasak et al., 1999), which defines the interpolation factors f_x for ϕ_f in Eq. (14) where

$$\phi_f = f_x \phi_P + (1 - f_x) \phi_N \quad (16)$$

and f_x is a general (non-linear) function of the face flux F , ϕ , its gradients and local geometry constructed according to the differencing scheme in such a way as to preserve boundedness.

The diffusive terms are treated similarly,

$$\oint_S \mathbf{ds} \cdot (\gamma \nabla \phi) \approx \sum_f \gamma_f \mathbf{s}_f \cdot \nabla \phi_f, \quad (17)$$

and are discretised either implicitly or explicitly, as follows:

- *Implicit discretisation.*

$$\mathbf{s}_f \cdot (\nabla \phi)_f = |\mathbf{o}| \frac{\Phi_N - \phi_P}{|\mathbf{d}_N|} + \mathbf{k} \cdot (\nabla \phi)_f. \quad (18)$$

Vectors \mathbf{o} and \mathbf{k} represent the non-orthogonal decomposition of the face area vector \mathbf{s}_f such that

$$\mathbf{s}_f = \mathbf{o} + \mathbf{k}, \quad (19)$$

where \mathbf{o} is parallel with \mathbf{d}_N (Jasak, 1996), Fig. 2. For all terms other than convection, the interpolation factor f_x is calculated from geometrical considerations

$$f_x = \frac{\overline{fN}}{\overline{PN}}. \quad (20)$$

- *Explicit discretisation.* $(\nabla \phi)_f$ is interpolated onto the face using Eqs. (16) and (20).

Using the above, the discretised transport equation takes the form

$$\frac{\phi - \phi^0}{\delta t} V_P + \sum_f F \phi_f - \sum_f \gamma_f \mathbf{s} \cdot (\nabla \phi)_f = S V_P + L V_P \phi_P. \quad (21)$$

Assembling Eq. (21) as described above produces

$$a_P \phi_P + \sum_N a_N \phi_N = r_P \quad (22)$$

with one equation assembled for each CV. a_P and r_P include contributions from the temporal term, source terms and boundary conditions. Here ϕ_P depends on the values in the neighbouring cells (ϕ_N), thus creating a system of linear algebraic equations

$$[A][\phi] = [r], \quad (23)$$

where $[A]$ is a sparse diagonally dominant matrix, with coefficients a_P on the diagonal and a_N off the diagonal, $[\phi]$ is the vector of ϕ s for all CVs and $[r]$ is the right-hand side vector.

Evaluation of the gradient. The cell centre gradient is calculated using a least-square fit (Jasak and Weller, 2000; Demirdžić and Muzaferija, 1995) in the following way: consider the cell P and the set of its neighbours N . Assuming a linear variation of ϕ around P , the error in the “shape function” at point N is

$$e_N = \phi_N - (\phi_P + \mathbf{d}_N \cdot (\nabla\phi)_P). \quad (24)$$

Minimising $e_P^2 = \sum_N (w_N e_N)^2$ ($w_N = \frac{1}{|\mathbf{d}_N|}$ is the weighting function) leads to the following expression

$$(\nabla\phi)_P = \sum_N w_N^2 \mathbf{G}^{-1} \cdot \mathbf{d}_N (\phi_N - \phi_P), \quad (25)$$

where \mathbf{G} is a 3×3 symmetric matrix

$$\mathbf{G} = \sum_N w_N^2 \mathbf{d}_N \mathbf{d}_N. \quad (26)$$

This produces a second-order accurate gradient irrespective of the arrangement of the neighbouring points. Moreover, the matrix \mathbf{G} can be inverted only once and stored to increase computational efficiency.

The above discretisation can now be used either implicitly (i.e. involving matrix inversion) or explicitly, depending on the characteristics of the algorithm. For more details on the FV discretisation the reader is referred to Hutchings (2000), Ferziger and Perić (1995), Jasak (1996) and Hirsch (1991).

Treatment of non-linear and coupling terms. The FVM is typically used in conjunction with several numerical practices. First, the matrices resulting from the discretisation are sparse and diagonally dominant, allowing the use of efficient sparse matrix iterative solvers. In this study, we shall use the conjugate gradient method with incomplete Cholesky preconditioning (ICCG) (Hestens and Steifel, 1952; Van Der Vorst, 1992). Coupled and vector equations are typically solved in a segregated manner, where each variable or vector component is solved separately and the coupling is ensured through the algorithm.

The discretised system includes some explicit (coupled) terms, depending on the solution from the previous iteration. It would therefore be unnecessary to converge the solution of Eq. (23) to a very tight tolerance, as the new solution will only be used to update the explicit terms. Only when the solution changes less than some predefined tolerance is the system considered to be solved. In transient calculations, this is performed for every time-step, using the previously available solution as the initial guess. The combination of iterative solvers, partial convergence and segregated discretisation results in an efficient solution strategy for non-linear problems, provided the non-linear interaction is treated in an appropriate way, which is our task in the remainder of this paper.

Boundedness. In physical models there typically exist a set of variables with physical bounds, for example negative values of thickness or a ice area fraction below zero or higher than unity are meaningless. The model is set up such that unphysical values cannot occur. An important role of good discretisation is to preserve the physical bounds of bounded variables in the discretised form.

From the boundedness point of view, the FVM can preserve the physical bounds of the variable provided three criteria are satisfied:

- A bounded convection differencing scheme is used. This subject has been analysed in depth in the FVM literature (see e.g. Ferziger and Perić, 1995); in this study we use the Gamma differencing scheme (Jasak et al., 1999).
- The source terms are discretised such that the term becomes implicit as the variable approaches its bound.
- It is algorithmically guaranteed that the iteration sequence towards the converged solution does not create unphysical intermediate solutions.

The importance of boundedness in the sea ice model will be examined further in Section 4.1.

Mesh structure. As mentioned before, a FV mesh consists of arbitrary polyhedra bounded by flat polygons (in 3-D) and is by no means limited to hexahedral elements or alignment with some coordinate system. This kind of mesh structure gives considerable freedom in mesh generation (e.g. the mesh may be fitted to follow the actual coastline instead of approximating it by a castellated surface) and allows the use of embedded mesh refinement (Ferziger and Perić, 1995; Jasak and Gosman, 2000) in regions where higher resolution is needed (e.g. Canadian Archipelago). Interesting avenues of future research include investigating the effect of more detailed coastline description on the overall model behaviour and modelling ice export through the Canadian Archipelago.

4. Analysis of the model

In this section we compare the viscous-plastic sea ice model with two similar numerical models widely simulated in the engineering community: a compressible fluid flow of an ideal gas and a linear elastic solid stress model. We are particularly interested in the form of the stress term and the interaction between the continuity and the momentum equation. For reference, the two models are summarised below. These models are written with traditional notation, introducing some notation clashes which are limited to this section.

Compressible fluid flow model of an ideal gas

$$\frac{\partial \rho}{\partial t} + \nabla \cdot (\rho \mathbf{u}) = 0, \quad (27)$$

$$\frac{\partial (\rho \mathbf{u})}{\partial t} + \nabla \cdot (\rho \mathbf{u} \mathbf{u}) - \nabla \cdot (\mu \nabla \mathbf{u}) = -\nabla p + \nabla \mu \cdot \nabla \mathbf{u} + \mu \nabla (\nabla \cdot \mathbf{u}), \quad (28)$$

$$\frac{\partial (\rho e)}{\partial t} + \nabla \cdot (\rho \mathbf{u} e) - \nabla \cdot \left(\frac{\mu}{Pr} \nabla e \right) = p \nabla \cdot \mathbf{u} + \Phi, \quad (29)$$

where ρ is the fluid density, related to the pressure p as $p = \rho RT$, \mathbf{u} is the velocity, e is the internal energy: $e = C_v T$, Pr is the Prandtl number and Φ is the viscous dissipation. The definition of the viscous stress tensor used above is

$$\boldsymbol{\sigma} = \mu [\nabla \mathbf{u} + (\nabla \mathbf{u})^T] - \mathbf{I} \left(\frac{2}{3} \mu \nabla \cdot \mathbf{u} + p \right), \quad (30)$$

where μ is the dynamic viscosity.

Linear elastic solid model

$$\frac{\partial^2(\rho \mathbf{d})}{\partial t^2} - \nabla \cdot \boldsymbol{\sigma} = \rho \mathbf{f}, \tag{31}$$

$$\boldsymbol{\sigma} = 2\mu\boldsymbol{\epsilon} + \lambda \text{tr}(\boldsymbol{\epsilon})\mathbf{I}, \tag{32}$$

$$\boldsymbol{\epsilon} = \frac{1}{2}[\nabla \mathbf{d} + (\nabla \mathbf{d})^T], \tag{33}$$

where \mathbf{d} is the displacement vector, ρ is the density, \mathbf{f} is the body force, $\boldsymbol{\sigma}$ is the stress tensor, $\boldsymbol{\epsilon}$ is the strain tensor and μ and λ are the Lamé’s coefficients, relating to the Young’s modulus of elasticity E and the Poisson’s ratio ν as

$$\mu = \frac{E}{2(1 + \nu)}, \tag{34}$$

$$\lambda = \begin{cases} \frac{\nu E}{(1+\nu)(1-\nu)} & \text{for plane stress,} \\ \frac{\nu E}{(1+\nu)(1-2\nu)} & \text{for plane strain.} \end{cases} \tag{35}$$

Using the above, the governing equation can be rewritten with the displacement vector \mathbf{d} as the primitive variable

$$\frac{\partial^2(\rho \mathbf{d})}{\partial t^2} - \nabla \cdot [\mu \nabla \mathbf{d} + \mu (\nabla \mathbf{d})^T + \lambda \text{Itr}(\nabla \mathbf{d})] = \rho \mathbf{f} \tag{36}$$

and the stress tensor reads

$$\boldsymbol{\sigma} = \mu[\nabla \mathbf{d} + (\nabla \mathbf{d})^T] + \lambda \text{Itr}(\nabla \mathbf{d}). \tag{37}$$

4.1. Physical bounds in the Hibler model

We can make some a priori statements regarding the behaviour of the Hibler model. For example, it is clear the ice thickness h cannot become negative and the ice fraction A is bounded between 0 and 1. During physical modelling, the source terms (S_h and S_A) need to be constructed such that the above bounds are preserved; it is our task to enforce the same criterion on the discretised form. If this is not the case, h and A bounds would need to be artificially imposed, e.g. by “clipping” the variables. This in turn would represent an arbitrary source/sink in the equation and severely degrade the accuracy of the solution.

From a modelling point of view, boundedness is achieved by requiring the source terms to go to zero as the variable approaches its bounds; the convective and diffusive transport on their own are unable to create any new extrema and as such do not feature in the boundedness analysis. Numerically, the bounds are enforced by an appropriate implicit/explicit source treatment and algorithmic features. For example, sink terms are treated implicitly if the variable is bounded below by zero, and L from Eq. (10) becomes a part of the a_P coefficient (Patankar, 1981).

4.2. Form of the stress term

A second interesting point is the form of the stress term, Eq. (2): the first part of the term is very similar to the stress of linear elastic solid model (taking into account the difference between the

displacement \mathbf{d} in Eq. (37) and the velocity \mathbf{u} in Eq. (2)), whereas the second part looks like the pressure term in the fluid model.

Consider the similarity between the ice thickness equation, Eq. (6) and the density equation in the compressible gas model, Eq. (27). Both express continuity of mass and both ρ and h are bounded below by zero. In the case of a compressible gas, the pressure term (a part of the stress tensor modelling) is explicitly stated in the momentum equation. This “pressure–velocity” combination is central to “pressure-based” compressible flow algorithms (e.g. Demirdžić et al., 1993), which are shown to be stable, bounded and accurate. The basis of the algorithm is the fact that the density can be represented in terms of pressure

$$\rho = \psi p, \quad (38)$$

where ψ is the compressibility and the pressure gradient term appears in the momentum equation.

Looking at Eqs. (1) and (8), we can achieve the same effect for the Hibler model. Given Eq. (8) h may be expressed as a function of P

$$h = \psi p, \quad (39)$$

where

$$\psi = \frac{2\rho_i}{P^\star e^{-C(1-A)}} \quad (40)$$

and

$$p = \frac{P}{2\rho_i}. \quad (41)$$

Dividing the momentum equation by the density of ice, ρ_i , and rewriting the viscosities as $\eta' = \frac{\eta}{\rho_i}$ and $\zeta' = \frac{\zeta}{\rho_i}$,

$$\frac{\partial(h\mathbf{u})}{\partial t} + \nabla \cdot (h\mathbf{u}\mathbf{u}) - \nabla \cdot [\eta'(\nabla\mathbf{u} + (\nabla\mathbf{u})^T) + (\zeta' - \eta')\mathbf{Itr}(\nabla\mathbf{u})] = -\nabla p + \mathbf{F}. \quad (42)$$

We can now perform the transformation of the ice thickness equation into the pressure equation. A solution algorithm is then developed, from experience of solving the compressible fluid model.

4.3. Variation in the speed of sound

Recognising the fact that the Hibler model, in its characteristics, is very similar to that of an ideal gas, we can consider the form of the stress term, Eqs. (2)–(4) and (8), from the point of view of the speed of sound. For packed ice ($A \rightarrow 1$) and inside the yield curve, the compressibility is low and the transfer of information about the stress state is close to elliptic—this would be similar to weakly compressible fluids (e.g. water), where the pressure term becomes almost elliptic in nature. However, when the stress state reaches the yield curve or the area fraction becomes low ($A \rightarrow 0$), the compressibility becomes very high, resulting in a low speed of sound. In a typical simulation, regions of the packed ice coexist with regions of open water and the robust numerical algorithm needs to take into account the large range in the speed of propagation of stress information through the medium. This is easily achieved by reformulating the ice thickness equation into the pressure equation and is equivalent to a similar solution methodology for compressible gas flows.

4.4. Equation coupling

In comparison with fluid flow models the inter-equation coupling in the Hibler model is remarkably complex. However, experience shows that the most efficient way of solving highly non-linear problems of this kind (yielding plastic material) is a segregated solution procedure, where each equation is solved separately and the coupling is ensured with an appropriate algorithmic setup. The coupling in the system is mainly twofold. First, the momentum equation is strongly coupled with the ice thickness equation, as the ice thickness determines the strength in the ice interaction terms. Also, the boundedness of the ice thickness equation crucially depends on the ice velocity field satisfying the ice continuity equation. Second, the components of the ice velocity vector are coupled more strongly than in fluid flows. In order to justify this statement, we need to compare the stress terms in the two reference models shown above. In fluids the $\nabla \cdot \boldsymbol{\sigma}$ term degenerates as the speed of sound approached infinity ($\psi \rightarrow 0$), or $\nabla \cdot \mathbf{u} \rightarrow 0$, as follows

$$\begin{aligned} \nabla \cdot \boldsymbol{\sigma} &= \nabla \cdot \left[\mu[\nabla \mathbf{u} + (\nabla \mathbf{u})^T] + \left(\frac{2}{3} \text{tr}(\nabla \mathbf{u}) - p \right) \mathbf{I} \right] \\ &= \nabla \cdot (\mu \nabla \mathbf{u}) + \nabla \mu \cdot \nabla \mathbf{u} + \mu \nabla (\nabla \cdot \mathbf{u}) + \nabla \left(\frac{2}{3} \nabla \cdot \mathbf{u} - p \right) \\ &\approx \nabla \cdot (\mu \nabla \mathbf{u}) + \nabla \mu \cdot \nabla \mathbf{u} - \nabla p. \end{aligned} \tag{43}$$

From the above it can be seen that the $\nabla \cdot (\nabla \mathbf{u})^T$ term (which represents the cross-component coupling) scales with the viscosity gradient and is typically low. In the linear elastic solid model, the importance of the $\nabla \cdot (\nabla \mathbf{d})^T$ term is equal or greater than that of the $\nabla \cdot (\nabla \mathbf{d})$ term, implying that the x -component of displacement in a cell is equally dependent on both the x - and y -displacement components of its neighbours, representing “strong cross-component coupling”. Jasak and Weller (2000) show that sufficiently strong coupling for such systems can be achieved by decomposing the stress tensor such that the explicit part represents pure rotation

$$\begin{aligned} \nabla \cdot \boldsymbol{\sigma} &= \underbrace{\nabla \cdot (\mu \nabla \mathbf{u})}_{\text{implicit}} + \underbrace{\nabla \cdot [\mu(\nabla \mathbf{u})^T + \lambda \mathbf{I} \text{tr}(\nabla \mathbf{u})]}_{\text{explicit}} \\ &= \underbrace{\nabla \cdot [(2\mu + \lambda) \nabla \mathbf{u}]}_{\text{implicit}} + \underbrace{\nabla \cdot [\mu(\nabla \mathbf{u})^T + \lambda \mathbf{I} \text{tr}(\nabla \mathbf{u}) - (\mu + \lambda) \nabla \mathbf{u}]}_{\text{explicit}}. \end{aligned} \tag{44}$$

Assuming $\mu, \lambda = \text{const.}$, the explicit part of the second form in Eq. (44) can be written as $\nabla \cdot [(\mu + \lambda)(\nabla \mathbf{d} - (\nabla \mathbf{d})^T)]$, which indeed represents rotation. In the rest of this paper we refer to the first form in Eq. (44) as “standard coupling” and the second as “strongly implicit coupling”.

In the next section we present the new form of the discretised Hibler model by combining the practices described above. The main points are the segregated solution algorithm, the formulation of the ice strength equation from the ice thickness equation and the implicit–explicit split of the stress terms such that only pure rotation is treated explicitly.

5. Discretised form of the sea ice model

In this section a new iterative procedure for the viscous-plastic sea ice model is introduced. This method requires the derivation of a transport equation for ice strength which utilises the

discretised–linearised form of the momentum equation. Discretisation of the new ice strength equation and updated momentum equation is performed in the same manner as described in Section 3.

5.1. Derivation of the transport equation for ice strength

Given Eq. (8), h may be expressed as a function of the ice strength p , Eq. (39)

$$h = \psi p,$$

where ψ is the effective compressibility. Eq. (42) is rewritten in the strongly implicit form (see Eq. (44))

$$\frac{\partial(h\mathbf{u})}{\partial t} + \nabla \cdot (h\mathbf{u}\mathbf{u}) - \nabla \cdot [(\eta' + \zeta')\nabla\mathbf{u}] = -\nabla \cdot [\eta'\nabla\mathbf{u}^T + (\zeta' - \eta')\mathbf{I}\text{tr}(\nabla\mathbf{u}) - \zeta'\nabla\mathbf{u}] + \mathbf{F} - \nabla p. \quad (45)$$

In the above equation, all the terms on the l.h.s. are treated implicitly and the r.h.s. terms are treated as linearised sources, Eq. (10).

In order to construct the continuity equation in terms of ice strength, Eq. (45) is discretised without the ∇p term. The discretisation follows that described in Section 3 using a forward Euler time step and semi-implicit treatment of ice velocity (see Section 4.4). The partially linearised and discretised momentum equation takes the form

$$a_p \mathbf{u}_p = \mathbf{H}(\mathbf{u}) - \nabla p, \quad (46)$$

where a_p is a diagonal coefficient and $\mathbf{H}(\mathbf{u})$ represents the off-diagonal discretisation coefficients a_N and the source terms

$$\mathbf{H} = \sum_N a_N \mathbf{u}_N + \mathbf{r}. \quad (47)$$

Note that the forcing term \mathbf{F} is fully contained in \mathbf{H} and a_p but the ice strength term is notionally left out. The above equation may be rewritten as

$$\mathbf{u}_p = \frac{\mathbf{H}(\mathbf{u})}{a_p} - \frac{1}{a_p} \nabla p. \quad (48)$$

Substituting Eqs. (39) and (48) into Eq. (6) gives a transport equation for p

$$\frac{\partial(\psi p)}{\partial t} + \nabla \cdot \left[\frac{\mathbf{H}(\mathbf{u})}{a_p} \psi p \right] - \nabla \cdot \left[\frac{h}{a_p} \nabla p \right] = S_h. \quad (49)$$

Here $\nabla \cdot \left[\frac{\mathbf{H}(\mathbf{u})}{a_p} \psi p \right]$ is an advection term, where $\frac{\mathbf{H}(\mathbf{u})}{a_p} \psi$ is the effective flux representing the information transfer based on the local speed of sound, dominating in loosely packed ice. The third term on the l.h.s. captures the elliptic effects of the stress transfer, which dominates in packed ice (low compressibility gives high speed of sound), thus covering the complete range.

An advantage of the strength equation method is that the ice mass flux term $F = \mathbf{s}_f \cdot \mathbf{u}_f h_f$ is available from the solution and the ice transport equation, Eq. (6), is automatically satisfied, as the ice strength equation, Eq. (49), has been derived from it. Thus, the additional numerical cost of solving the strength equation is counterbalanced by the fact the ice thickness is now automatically available, as will be shown in the following section.

Using the above procedure, the effects of the momentum transfer (previously completely contained in the momentum equation) have been split between the momentum, which resolves the advective ice transport and caters for the non-linearity of the stress term and cross-component coupling and the ice strength equation, which encompasses the “speed of sound” effects of the stress transfer through the ice. This split ensures that the elliptic (or nearly elliptic) effects are captured well even if the momentum equation is not fully converged. This practice has been proven to be effective in many pressure-based subsonic/transonic/supersonic flow algorithms, see for example Demirdžić et al. (1993) and Ferziger and Perić (1995).

5.2. Boundary conditions

The appropriate boundary conditions must be considered for open (ocean) and closed (land) boundaries. At ocean boundaries the velocity is set to have no gradient, at land boundaries the velocity is set to zero. Ice thickness h and area A are set to be gradient free at the ocean boundaries.

6. Iterative solution method

We now describe the solution methodology for two algorithms based on the FV discretisation described above. The first (“strength explicit”) will mimic the behaviour of the Zhang and Hibler (1997) numerics in the FV implementation and the second (“strength implicit”) will introduce the ice strength equation as described above.

6.1. Strength explicit algorithm

The solution sequence for the strength explicit algorithm is as follows:

1. Calculate the forcing field and growth/melt rates for the current time-step.
2. Calculate ζ' , η' and p based on the available solution (\mathbf{u}, h, A) .
3. Solve the momentum equation, Eq. (45)

$$\frac{\partial(h\mathbf{u})}{\partial t} + \nabla \cdot (h\mathbf{u}\mathbf{u}) - \nabla \cdot [(\eta' + \zeta')\nabla\mathbf{u}] = -\nabla \cdot [\eta'\nabla\mathbf{u}^T + (\zeta' - \eta')\mathbf{I}\text{tr}(\nabla\mathbf{u}) - \zeta'\nabla\mathbf{u}] + \mathbf{F} - \nabla p.$$

This equation is solved in a segregated manner (component by component) and the cross-component terms are lagged.

4. Repeat steps 2 and 3 until the convergence tolerance on the momentum equation is reached.
5. Given the final velocity field, calculate the flux terms using the interpolated velocity

$$F = \mathbf{s}_f \cdot \mathbf{u}_f. \tag{50}$$

6. Solve the ice transport equations, Eqs. (6) and (7) using the fluxes from Eq. (50)

$$\frac{\partial h}{\partial t} + \nabla \cdot (h\mathbf{u}) = S_h,$$

$$\frac{\partial A}{\partial t} + \nabla \cdot (A\mathbf{u}) = S_A.$$

Note that the boundedness of h now depends on the convergence threshold of the coupled system, which is clearly undesirable.

7. Proceed to the following time-step.

In order to achieve convergence of the above algorithm it is necessary to use the strongly implicit coupled form of stress discretisation, Eq. (45); without it (Eq. (42)), the iteration over the momentum equation is not convergent. It will be illustrated in Section 8 that the strongly coupled form of the stress term (see Eq. (44)) improves convergence of the momentum coupling.

The explicit flux calculation, Eq. (50) regularly gives rise to unbounded values of h , which need to be artificially clipped at their bounds. An additional iteration loop over the whole equation set was attempted within every time-step, but was found not to have any effect on the boundedness or accuracy of the procedure.

This is a typical example of unphysical intermediate solutions in the iteration loop: once the convergence is reached over the h – \mathbf{u} system, h would be bounded; however, as we cannot control the intermediate ice velocity solution with respect to h , Eq. (6) may produce negative intermediate values, with undesirable effects. Interference with the h field (“clipping”) inside the solution sequence violates mass conservation and distorts the final result.

6.2. Strength implicit algorithm

The solution sequence for the strength implicit algorithm is loosely based on the PISO pressure–velocity coupling algorithm (Issa, 1986). The PISO algorithm is set up to achieve efficient coupling between the pressure and momentum in fluid flows and can be modified for our purposes as follows:

1. Calculate the forcing field and growth/melt rates for the current time-step.
2. Using the flux field from the previous time-step, calculate the predicted ice thickness distribution

$$\frac{\partial h}{\partial t} = S_h - \nabla \cdot (h\mathbf{u}). \quad (51)$$

Note that the ice mass flux $F_h = \mathbf{s}_f \cdot \mathbf{u}_f h_f$ is already known from the previous strength solution, and Eq. (51) can be solved directly

$$h = h^0 + \delta t [S_h - \nabla \cdot (h\mathbf{u})] = h^0 + \delta t \left(S_h - \frac{1}{V_P} \sum_f F_h \right). \quad (52)$$

3. Solve the ice area transport, Eq. (7), using the area flux $F = \frac{F_h}{h_f}$

$$\frac{\partial A}{\partial t} + \nabla \cdot (A\mathbf{u}) = S_A.$$

4. Solve the ice strength–momentum equations using the Strength Implicit MOmentum correction (SIMON) algorithm:

- (a) Calculate ζ' and η' based on the available solution (\mathbf{u}, h, A) .
 (b) Formulate and solve the momentum predictor using the latest ice strength field p (the solution of Eq. (49) from the previous iteration), Eq. (45)

$$\frac{\partial(h\mathbf{u})}{\partial t} + \nabla \cdot (h\mathbf{u}\mathbf{u}) - \nabla \cdot [(\eta' + \zeta')\nabla\mathbf{u}] = -\nabla \cdot [\eta'\nabla\mathbf{u}^T + (\zeta' - \eta')\mathbf{Itr}(\nabla\mathbf{u}) - \zeta'\nabla\mathbf{u}] + \mathbf{F}. \quad (53)$$

- (c) Formulate and solve the ice strength equation, Eq. (49)

$$\frac{\partial(\psi p)}{\partial t} + \nabla \cdot \left[\frac{\mathbf{H}(\mathbf{u})}{a_p} \psi p \right] - \nabla \cdot \left[\frac{h}{a_p} \nabla p \right] = S_h.$$

This equation is discretised and linearised in a similar manner to the momentum equation. Discretisation is semi-implicit in p , with the diffusive term implicitly discretised as in Section 3. $\mathbf{H}(\mathbf{u})$, a_p and h are taken from the most recent discretisation of Eq. (45) and most recent solution for h , either Eq. (39) or Eq. (52).

- (d) Correct the velocity field with the new p using Eq. (48)

$$\mathbf{u}_p = \frac{\mathbf{H}(\mathbf{u})}{a_p} - \frac{1}{a_p} \nabla p.$$

The same equation (on the face) is used to calculate the face mass flux F from the new solution. Note that F will be conservative, as Eq. (49) has been derived directly from Eq. (6). If necessary, this step can be repeated several time, updating the $\mathbf{H}(\mathbf{u})$ term, Eq. (47), in every iteration.

- (e) Repeat the procedure until the momentum convergence tolerance is reached. A converged mass–momentum solution is obtained by iterating over the strength equation and the two momentum components.
 (f) At the end of the iteration the ice thickness is recalculated from the updated ice strength field, Eq. (39)

$$h = \psi p.$$

5. Proceed to the following time-step.

The crucial point in the algorithm is the explicit correction of ice velocity based on the ice strength, Eq. (49): this guarantees that the ice thickness field calculated using Eq. (52) always remains bounded.

Finally, a word on extending the strength implicit algorithm to other sea ice models. The procedure described above relies on the fact that there exists an equation for the total mass of ice per unit area and the distribution into thickness brackets is done separately. The derivation of the ice strength equation, the basis of this algorithm, can be done irrespective of the form of the rheology. A “numerics-friendly” way of describing ice thickness distribution would rely on the transport of its higher moments of thickness distribution rather than on thickness brackets. To summarise, the two requirements for the application of the strength implicit algorithm to an arbitrary rheology are: (i) the presence of an equation for the total ice mass per unit area (i.e. thickness h or integrated volume from a thickness distribution function) and (ii) the possibility of expressing the spherical part of the ice stress tensor as a (potentially non-linear) function of ice mass per unit area.

7. Case study

A simple case study of convergent ice flow against a shore demonstrates the importance of resolving ice strength–velocity coupling and the boundedness of the ice transport terms. The test setup is as follows: ice on a stationary, flat ocean is forced with a constant wind at an angle of 30° towards the coast. The wind stress is modelled with a quadratic drag law (Brown, 1979) and the thermodynamic sources of ice are set to zero. The one-dimensional problem may be solved analytically (Leppranta and Hibler, 1985) for the ice thickness gradient. For numerical solution the spatial domain is split into a 40 km resolution 30 by 10 rectangular grid, with land boundary conditions for the short boundary onto which the ice is blown and ocean boundary conditions for the other three boundaries.

Numerical solutions for ice thickness are obtained with the two methods described above. Both methods use identical discretisation schemes and time stepping, with 20 iterations over the momentum coupling within each time step; the only difference being the treatment of the ice strength term in the momentum equation. In both numerical solutions we find, as expected, the ice thickness only varies in the direction towards the coast.

The evolution of the transient solution is shown in Fig. 3 for both numerical solutions. Eventually the ice thickness gradient for both runs is close to that calculated analytically. Without ice strength corrections a grid point instability is introduced in the mass field, though the velocity field is smooth.

This grid point instability is indicative of an unconverged ice strength solution. The waves introduced in the thickness field are unphysical and hinder convergence to an equilibrium solution. There is a mass difference between the two numerical solutions, with a thickness difference of

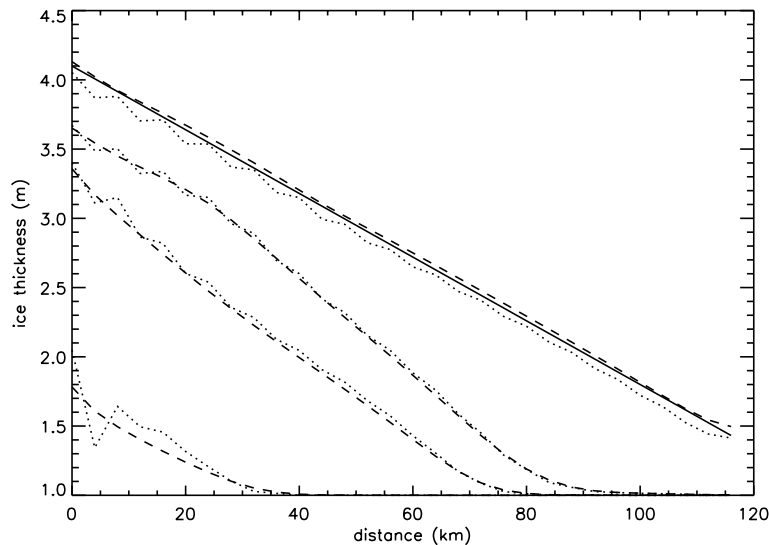


Fig. 3. The evolution of ice thickness is shown for the strength explicit (dotted lines) and strength implicit (dashed lines) solutions. Thickness profiles are plotted after 1 day, 1 month, 1 year and 200 years. The solid line represents the ice thickness gradient found from analytic solution.

0.1 m after 200 years. This is due to the accumulative effect of a small difference in velocity, and hence ice influx at the right hand boundary.

8. Convergence characteristics of the strength implicit algorithm

We now examine the difference between the standard form of the stress term discretisation, Eq. (42) and the strong cross-component coupling, Eq. (45). The analysis has been performed under a wide range of conditions (Hutchings, 2000), both with simple case studies and a realistic simulation of the Arctic sea ice as presented in Section 9. The results presented below are typical for the behaviour of the algorithm under realistic conditions.

Looking at the convergence of velocity, Fig. 4 it can be seen that the standard formulation is not convergent, whereas with the strongly implicit formulation, Eq. (45), about 20 iterations are required to reach a tolerance comparable with the errors in the numerical discretisation and less than ten iterations for a numerically acceptable solution. The performance of the strength implicit algorithm for this case, Fig. 5, shows a further improvement in convergence, due to the implicit treatment of ice strength.

In the original correction scheme (Zhang and Hibler, 1997) and the strength explicit method the majority of the computational cost occurs in solving the momentum equation. Transport equations with dominant advection terms are typically solved in 1 or 2 sweeps of the ICCG solver. In contrast, the momentum equation contains dominant diffusion terms, and is solved in about 20 iterations. The strength implicit scheme shifts the normal part of the stress into the p equation, substantially reducing the computational cost of solving the momentum equation (1 or 2 solver sweeps). The cost is transferred to the p equation, which due to the normal stress term, $\nabla \cdot \left[\frac{h}{ap} \nabla p \right]$, requires about 20 solver sweeps.

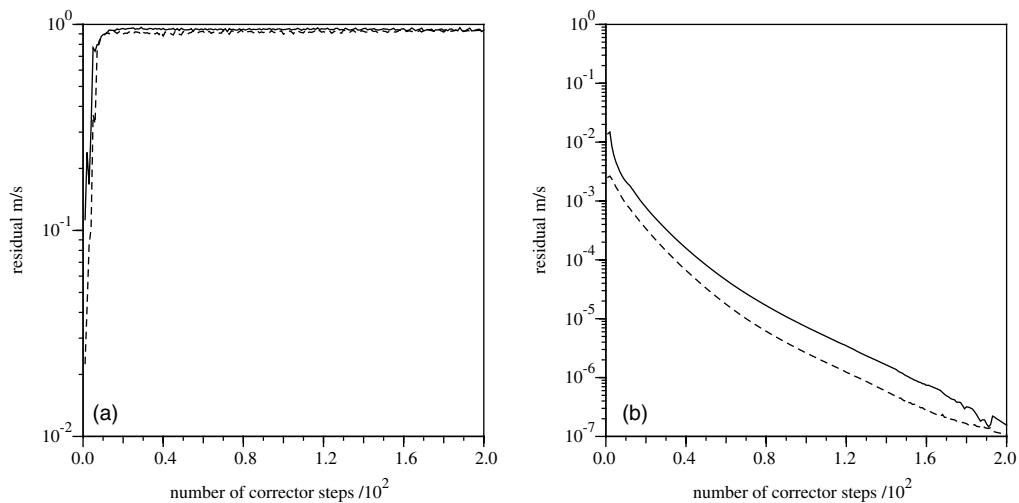


Fig. 4. Velocity residual plotted against number of ice strength correction iterations for the strength explicit algorithm. The convergence of u_x is shown as a solid line and u_y as a dashed line. (a) Standard stress term discretisation. (b) Strongly coupled stress term discretisation.

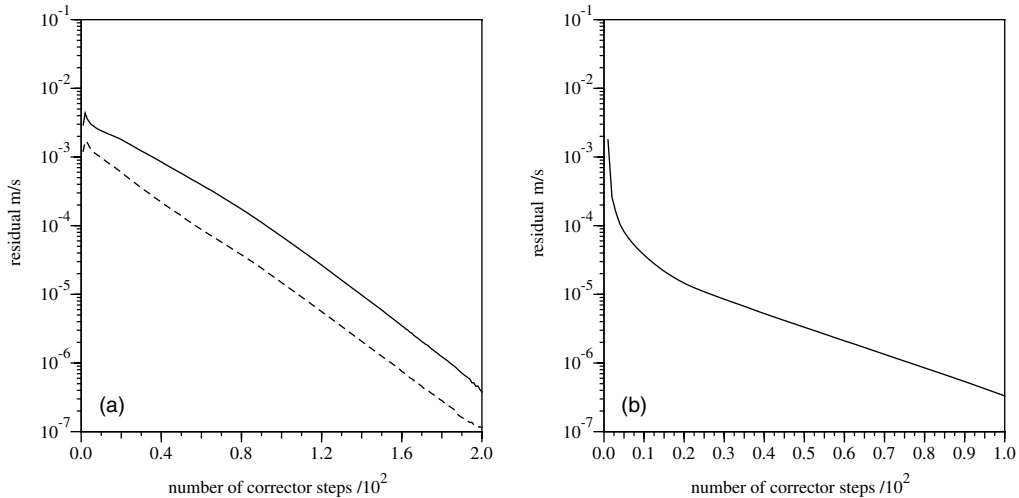


Fig. 5. Convergence of the strength implicit algorithm. (a) Velocity residual. (b) Ice strength residual.

The ice strength implicit algorithm has essentially the same computation cost as the strength explicit algorithm. For the model runs presented here CPU time is increased by less than 1% when the ice strength correction scheme is introduced. The important point to note is that the strength implicit scheme ensures a fully converged mass–momentum solution and provides a set of conservative ice mass fluxes for the same price as determining the converged velocity solution.

9. A simulation of Arctic sea ice

To investigate whether ice strength–velocity coupling is important in large scale simulations of Arctic sea ice, results are presented for two 10 year, 110 km resolution simulations of ice in the Arctic ocean. Both simulations were initialised after 20 years spin-up with Daily NCEP/NCAR reanalysis wind forcing (1979–1998), constant ocean forcing (a mean geostrophic current for 1992 taken from OCCAM (Webb et al., 1998)) and climatological ice growth/melt rates provided by Thorndike et al. (1975). The first simulation uses the strength explicit iterative method and in the second the strength implicit algorithm is used. Realistic ice drift patterns are reproduced in the Beaufort Sea in both models, but ice thickness in the GIN sea is unrealistic as the climatological growth/melt rates are not appropriate here. Even so, this model indicates how the errors due to unresolved mass–momentum coupling affect the simulated ice thickness in the Arctic Ocean, especially the Beaufort Sea where ice converges on the North American coast.

Fig. 6 shows a time series of the difference in total ice volume over a ten year time period. Notice that the strength implicit simulation has $3.5 \times 10^{12} \text{ m}^3$ less ice than the strength explicit solution after only six years. This mass difference is equivalent to a mean thickness difference of 30 cm and is introduced by the non-conservative nature of the strength explicit algorithm. The geographical difference in ice thickness between the two solutions, after 10 years of integration is shown in Fig. 7. There are substantial differences of over 40 cm in localised bands throughout the central Arctic. The thickness difference in the Western Arctic is an artifact of convergent flow

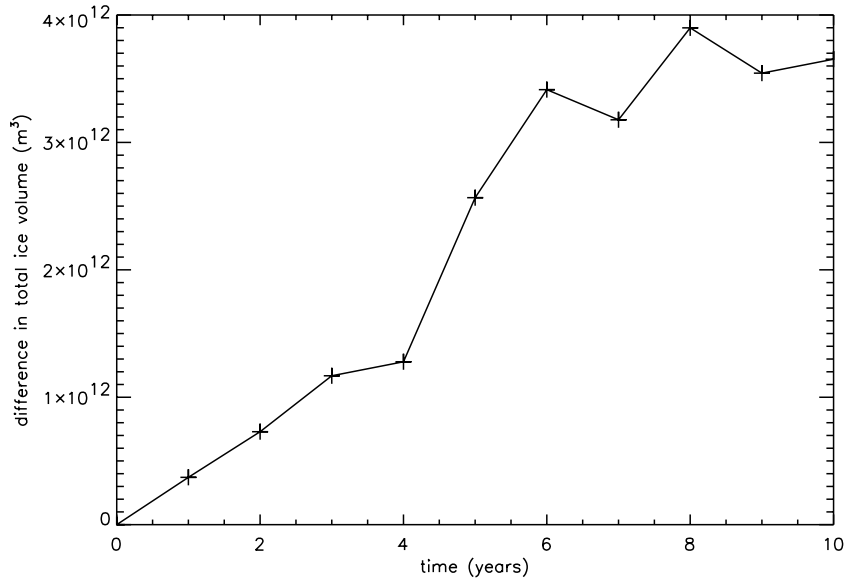


Fig. 6. Time series of total ice volume difference between the two simulations, strength explicit minus strength implicit.

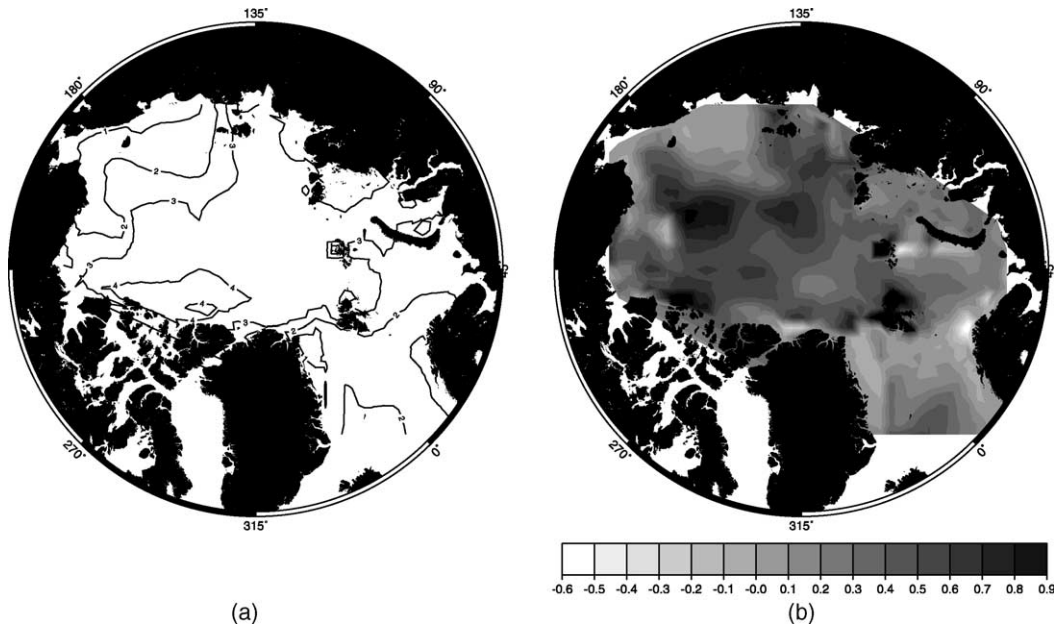


Fig. 7. (a) Ice thickness, in metres, for the strength explicit simulation and (b) thickness difference, in metres, (strength explicit minus strength implicit) between the two model runs after ten years of integration, December 31st 1989.

towards the Canadian Coast, which the model reproduces well. Ice thickness is increased by over 50 cm in localised regions in the strength explicit simulation.

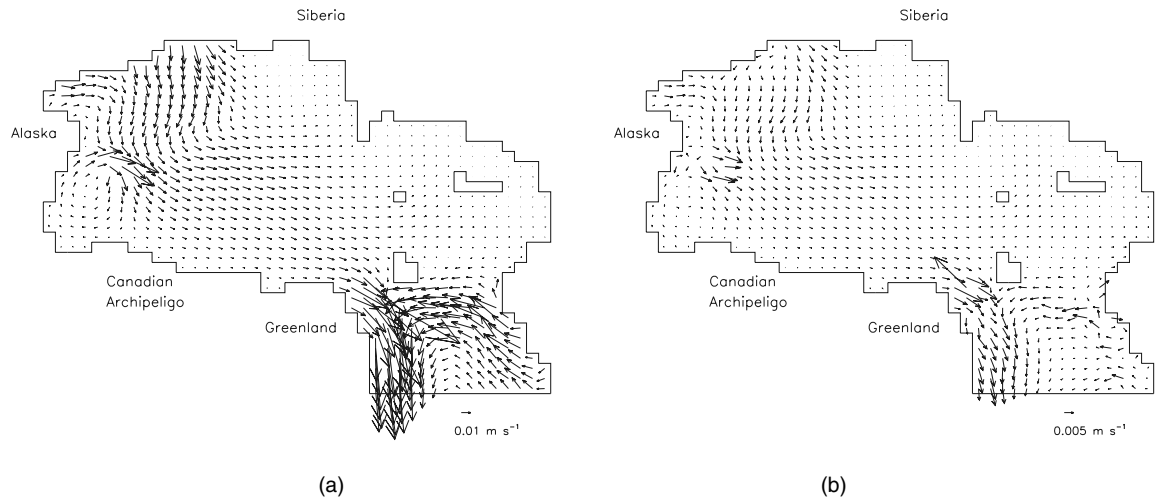


Fig. 8. (a) Mean ice velocity for the tenth year of the strength implicit simulation and (b) the difference in tenth year mean ice velocity between the two simulations. Note the scale difference between the two plots.

Note that the differences in ice velocity between the two Arctic simulations are small, Fig. 8. Ice export at Fram Strait and the Transpolar Drift is slightly increased in the strength implicit simulation. Fig. 9 show the mass budget for the first year of both simulations. The ice export to the North Atlantic is reduced and thermodynamic growth is enhanced in the strength explicit simulation. From Section 7 we know that without thermodynamics it takes many tens of years for an accumulative mass error to become significant. The source of ice mass due to numerical error is larger with the strength explicit method, Fig. 9d. The thickness error for the strength explicit method is $O(1 \times 10^{-2} \text{ m})$. Whereas the strength implicit thickness error, $O(1 \times 10^{-3} \text{ m})$, is comparable to the velocity error, Figs. 4 and 5. In the Arctic simulations significant differences in ice thickness appear within a year. Essentially it is small differences in ice velocity (export and convergence) between the two simulations, due to the initial thickness error, that amplifies the initial thickness difference. It should be noted that the velocity field is found to the same numerical tolerance in both simulations, see Section 8. It is the increased mass error in the strength explicit method that introduces the velocity differences. The strength implicit method ensures that a fully coupled mass–momentum solution is found with a continuity error that is comparable to the momentum error. The increased convergence in the strength explicit run results in thicker ice. For thicker ice, growth and melt rates are reduced, resulting in a longer growth season. This positive feedback between thermodynamics and dynamics causes remarkably different ice thickness fields in the two Arctic simulations.

Hutchings (2000) demonstrated that the strength explicit version of the viscous–plastic model overestimated ice thickness, compared to satellite altimetry estimates of ice thickness (Peacock, 1999), by up to three meters in the Beaufort Sea. The error introduced through not resolving ice strength–velocity coupling may account for 25% of the difference between model and observations.

An important point to note is that other sources of mass error, such as an imposed ice thickness cut-off, will behave in much the same fashion as the numerical error in the strength explicit algorithm. Thermodynamic–dynamic feedback causes small anomalies in ice mass to be amplified

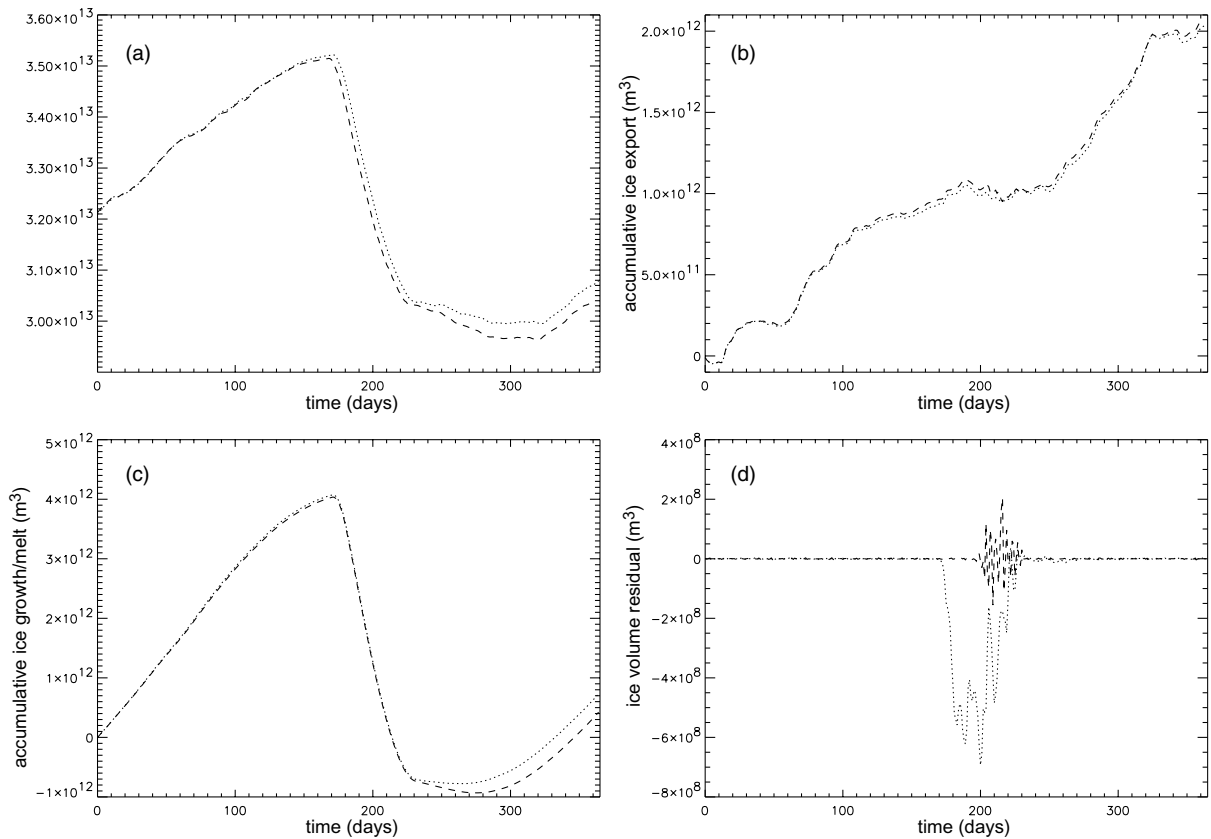


Fig. 9. Ice mass budget for first year of simulations. The strength explicit results are shown as dotted lines, strength implicit results as dashed lines: (a) shows the time series of total mass of ice in the model domain; (b) shows the accumulative ice export and (c) the accumulative thermodynamic source of ice over the year. The numerical error (d) is the residual of the mass budget, and does not include the artificial source due to ice thickness cut-off.

on yearly time scales. The strength explicit method requires a thickness cut-off for stability, whereas the strength implicit method does not. Essentially as the strength explicit method does not guarantee the velocity field is physical (as defined by continuity), undershoots in ice thickness may occur. In the presence of negative ice thickness the model is no longer well posed, and becomes unstable. We believe that accurate simulation of the ice mass balance is imperative, as small errors are amplified through non-linearities in the model. The strength implicit method ensures that the ice strength field is found such that it obeys continuity, ice strength–velocity coupling is well resolved and ice thickness determined to the same numerical tolerance as velocity.

10. Summary

This paper presented a new finite volume iterative solution algorithm for the viscous-plastic sea ice model which ensures ice strength–velocity coupling is well resolved. The contributions to the

solution methodology can be grouped into numerical and algorithmic issues. The main numerical characteristics of the model are

- stable, bounded and conservative finite volume discretisation, allowing greater accuracy and freedom in mesh generation;
- segregated solution algorithm with the use of sparse matrix iterative conjugate gradient solvers;
- strict conservation of ice mass and efficient treatment of non-linearity.

In order to achieve the above, the viscous-plastic rheology model (Hibler, 1979) has been examined and algorithmically reformulated with reference to the discretisation practices used in compressible gas and linear elastic solid models. Here, the main contributions are the reformulation of the stress tensor into a strongly implicit form and the derivation of the ice strength equation from the ice mass equation, separating the speed of sound effects from the momentum equation and treating them in an implicit manner. Coupling between the momentum and the ice strength equations is ensured algorithmically, through the strength implicit momentum correction treatment. The resulting model is shown to be convergent and bounded.

The strength implicit method ensures mass conservation is maintained through the ice strength field, and removes the need for lower cut-offs on ice mass entering the momentum equation. As the dominant coupling between mass and momentum is through the ice strength in the plastic constitutive law, explicit mass corrections to the momentum equation are not optimal. Without ensuring the ice strength field obeys continuity, a convergent ice strength–velocity solution can not be guaranteed. It was shown that the grid point ice thickness error due to unresolved ice strength–velocity coupling may become greater than 50 cm over several years of integration.

Acknowledgements

We would like to thank Henry Weller for his support in developing the finite volume sea ice model. The numerical results presented here were calculated with the aid of the FOAM object library for continuum mechanics (Weller et al., 1998; Nabla Ltd.). Many thanks to Bill Hibler for much discussion. The comments from three anonymous reviewers, Peter Killworth and Bob Prichard have all improved this paper. This work was funded with a Natural Environment Research Council PhD studentship.

References

- Bitz, C., Holland, A., Weaver, M., 2001. Simulating ice thickness distribution in a coupled climate model. *JGR* 106 (C2), 2441–2463.
- Brown, R., 1979. Planetary boundary layer modelling for AIDJEX. In: Pritchard, R. (Ed.), *Proc. ICSI/AIDJEX Symp. on Sea Ice Process and Models*, University of Washington, pp. 387–401.
- Demirdžić, I., Muzafrija, S., 1995. Numerical method for coupled fluid flow, heat transfer and stress analysis using unstructured moving meshes with cells of arbitrary topology. *Comput. Meth. Appl. Mech. Eng.* 109, 331–349.
- Demirdžić, I., Perić, M., Lilek, v., 1993. A collocated finite volume method for predicting flows at all speeds. *Int. J. Numer. Meth. Fluids* 16, 1029–1050.

- Ferziger, J., Perić, M., 1995. *Computational Methods for Fluid Dynamics*. Springer Verlag, Berlin, NY.
- Hestens, M., Steifel, E., 1952. Method of conjugate gradients for solving linear systems. *J. Res.* 29, 409–436.
- Hibler, W., 1979. A dynamic thermodynamic sea ice model. *J. Phys. Oceanogr.* 9, 815–846.
- Hirsch, C., 1991. *Numerical Computation of Internal and External Flows*. John Wiley & Sons.
- Hutchings, J.K., 2000. On modelling the mass of Arctic sea ice. PhD thesis, University of London.
- Hunke, E.C., Dukowicz, J.K., 1997. An elastic-viscous-plastic model for sea ice dynamics. *J. Phys. Oceanogr.* 27 (9), 1849–1867.
- Issa, R., 1986. Solution of the implicitly discretized fluid flow equations by operator-splitting. *J. Comput. Phys.* 62, 40–65.
- Jasak, H., 1996. Error analysis and estimation for the finite volume method with application to fluid flow. PhD thesis, Imperial College, University of London.
- Jasak, H., Gosman, A., 2000. Automatic resolution control for the finite volume method, part 2: Adaptive mesh refinement. *Numer. Heat Transfer, B* 38 (3), 257–272.
- Jasak, H., Weller, H., 2000. Application of the finite volume method and unstructured meshes to linear elasticity. *Int. J. Numer. Meth. Eng.* 48 (2), 267–287.
- Jasak, H., Weller, H., Gosman, A., 1999. High resolution NVD differencing scheme for arbitrarily unstructured meshes. *Int. J. Numer. Meth. Fluids* 31, 431–449.
- Kaluderčić, B., 2000. Parallelisation of Eulerian and Lagrangian CFD algorithms. PhD thesis, University of London.
- Kreyscher, M., Harder, M., Lemke, P., Flato, G.M., 2000. Results of the sea ice model intercomparison project: evaluation of sea ice rheology schemes for use in climate simulations. *JGR* 105 (C5), 11299–11320.
- Lemke, P., Heygster, G., Toudal, L., Turner, J., 1998. SEa ice in the Antarctic LInked with OceaN-atmosphere forcing. In: *Proceedings of the European Climate Science Conference*, pp. 19–23.
- Leppranta, M., Hibler, W.D., 1985. The role of plastic ice interaction in marginal ice zone dynamics. *JGR* 90 (C6), 11899–11909.
- Oberhuber, J.M., 1993. Simulation of the Atlantic circulation with a couple sea ice–mixed layer–isopycnal general circulation model. Part I: model description. *J. Phys. Oceanogr.* 23, 808–829.
- Patankar, S., 1981. *Numerical Heat Transfer and Fluid Flow*. Hemisphere Publishing Corporation.
- Peacock, N., 1999. Arctic sea ice and ocean topography from satellite altimetry. PhD thesis, University College London, University of London.
- Thorndike, A., Rothrock, D., Maykut, G., Colony, R., 1975. The thickness distribution of sea ice. *JGR* 80 (33), 4501–4513.
- Van Der Vorst, H., 1992. Bi-CGSTAB: A fast and smoothly converging variant of Bi-CG for the solution of nonsymmetric linear systems. *SIAM J. Sci. Comput.* 13 (2), 631–644.
- Webb, D., de Cuevas, B., Coward, A., 1998. The first main run of the occam global ocean model. Technical Report 34, Southampton Oceanography Centre, Southampton University, UK.
- Weller, H., Tabor, G., Jasak, H., Fureby, C., 1998. A tensorial approach to computational continuum mechanics using object orientated techniques. *Comput. Phys.* 12 (6), 620–631.
- Zhang, J., Hibler, W., 1997. On an efficient numerical method for modeling sea ice dynamics. *JGR* 102 (C4), 8691–8702.